2026 Volume: 02 Issue: 04 www.ijrpa.com ISSN 2456-9995 Research Article

International Journal Research Publication Analysis

Page: 01-19

ENHANCING FREQUENCY STABILITY IN MULTI-AREA GRIDS WITH HIGH PENETRATION OF RENEWABLE ENERGY SOURCES

***Dahiru Zailani Lame, Kabiru Sani, D. M. Nazif**

Department of Electrical/Electronic Engineering Technology, Federal Polytechnic Bauchi, Bauchi State, Nigeria.

Article Received: 19 March 2026
Article Revised: 09 April 2026
Published on: 29 April 2026

***Corresponding Author: Dahiru Zailani Lame**
Department of Electrical/Electronic Engineering Technology, Federal Polytechnic Bauchi, Bauchi State, Nigeria.

DOI: https://doi-doi.org/101555/ijrpa.5021

ABSTRACT

The increasing integration of renewable energy sources into modern power systems poses significant challenges to frequency stability due to their intermittent and uncertain nature. This study focuses on enhancing frequency regulation in a two-area interconnected power system using advanced control strategies. A detailed Load Frequency Control (LFC) model was developed, incorporating the dynamics of the governor, turbine, generator, and tie-line to evaluate system response under load disturbances. Three control schemes were investigated: the conventional Integral controller, the Proportional-Integral-Derivative (PID) controller, and a Particle Swarm Optimization (PSO)-based PID controller. The PSO algorithm was employed to optimally tune the PID parameters by minimizing the Integral of Time-weighted Absolute Error (ITAE), thereby improving the dynamic performance of the system. Simulation results obtained from MATLAB/Simulink revealed significant performance differences among the controllers. The Integral controller recorded an overshoot of 0.0164, a settling time of 29.22 seconds, and an ITAE value of 2.2190, indicating slower response and poor damping characteristics. The conventional PID controller improved system performance with a reduced overshoot of 0.0026, a settling time of 29.98 seconds, and a lower ITAE value of 0.5194. However, the PSO-optimized PID controller demonstrated superior performance, achieving a minimal overshoot of 0.0007, the fastest settling time of 29.21 seconds, and the lowest ITAE value of 0.0557. These results indicate a substantial reduction in oscillations and improved system stability when PSO is applied. The PSO-PID controller provided the best dynamic response, exhibiting enhanced damping, faster stabilization, and improved robustness against disturbances. The study concludes that PSO-based optimization is an

effective approach for tuning controllers in multi-area power systems, particularly in the presence of renewable energy sources, and is recommended for practical implementation in modern power grid control.

KEYWORDS: LFC, PSO, PID, Multi-Area Power System, Frequency Stability, Renewable Energy Integration.

1.0 INTRODUCTION

Modern electric power systems are complex networks designed to ensure reliable generation, transmission, and distribution of electricity while maintaining a continuous balance between supply and demand (Mohanty, 2023). This balance is critical for system stability, as any mismatch leads to frequency deviations. Load Frequency Control (LFC) plays a vital role in regulating this balance by maintaining system frequency within acceptable limits (Abdelghany et al., 2024). In practice, constant fluctuations in load and generation cause frequency variations which, if not properly controlled, can degrade power quality, damage equipment, and even result in system instability or collapse (Roy & Oo, 2024; Khalil et al., 2022).

The complexity of LFC increases significantly in multi-area power systems, where multiple interconnected regions with different load and generation characteristics must operate in coordination (Daood et al., 2024). Although tie-lines improve reliability by enabling power sharing, they also allow disturbances to propagate across areas. For example, a sudden load change in one region can affect the entire network's frequency, necessitating coordinated control strategies (Aditya et al., 2024).

Conventional PID controllers are widely used in LFC due to their simplicity, but their performance depends heavily on precise tuning under nominal conditions, which rarely reflect real-world dynamics (Ali et al., 2025; Ahmed et al., 2021). The increasing variability in load demand, system nonlinearities, and especially the integration of renewable energy sources (RES) further limit their effectiveness (Alnefaie et al., 2025). Intelligent control techniques such as fuzzy logic, neural networks, genetic algorithms, and particle swarm optimization provide improved adaptability by handling uncertainties and nonlinear behaviors, thereby enhancing system stability and transient performance (Nath & Sambariya, 2023; Brahim et al., 2021; Reddy et al., 2024; Çavdar et al., 2024).

However, high penetration of RES introduces low-inertia conditions and power fluctuations that challenge traditional LFC methods (Rahman et al., 2023; Daood et al., 2024). Existing

centralized and some AI-based approaches often lack practical validation in hybrid, multi-source systems, leaving gaps in their real-world applicability (Khalil et al., 2022; Das et al., 2021). Additionally, there is a lack of adaptive frameworks that integrate decentralized and coordinated control across multiple areas, while issues such as scalability, RES variability, and limited research on energy storage roles further hinder the development of robust LFC systems (Doan et al., 2021; Dev et al., 2021; Hamza et al., 2022; Elkasem et al., 2024).

2.0 MATERIALS AND METHODS

2.1 Materials

The materials used in this research include a personal computer, Power system data, and the MATLAB software.

2.2 Methods

2.2.1 Dynamics of the Power System

Load frequency control (LFC) is a crucial process for large-sized generators, aiming to maintain unvarying frequencies, distribute loads, and manage tie line power exchange according to scheduled values. Various components of the automatic load frequency control loop are given away in Figure 1.

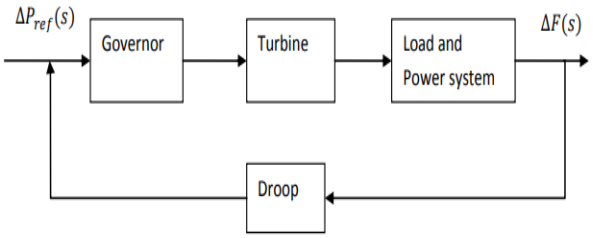

Figure 1: Block diagram of load frequency control (Doan et al., 2021).

2.2.2 Turbines

Turbines transform natural energy into mechanical power for generators and include three types: non-reheat, reheat, and hydraulic turbines (Wang et al., 2021). The model discussed illustrates how the power output of a non-reheat turbine reacts to variations in the steam valve's opening, incorporating a single gain factor KT and a single time constant T. In the model, the representation of the turbine is,

$$\frac{\Delta P_T(s)}{\Delta P_v(s)} = \frac{K_T}{1+sT_T} \quad \ldots(1)$$

Where, $\Delta P_v(s)$ = the input to the turbine; $\Delta P_T(s)$ =the output from the turbine

2.2.3 Generators

Generators convert mechanical power from turbines to electrical power, where the rotor speed is vital and directly proportional to the power system's frequency. It is crucial to balance generated power and load demands, as variations in load can lead to mechanical power exceeding generator power, resulting in frequency bias. Resistive loads (PL) can be fixed or can compensate for changes in load.

Mathematically,

$$\frac{\Delta P_v(s)}{\Delta P_g(s)} = \frac{K_T}{1+sT_g} \quad \ldots(2)$$

Where, $\Delta P_v(s)$ = the output from the generator, $\Delta P_g(s)$ = the input to the generator, $T_g(s)$ = time constant of the generator

2.2.4 Governors

Governors in power systems detect frequency bias due to load changes and eliminate it by altering turbine inputs, like speed regulation and governor time constant. LFC aims to limit frequency deviation in active power load, using the load reference set point to adjust valve/gate positions.

Mathematically,

$$\Delta P_g(s) = \Delta P_{ref}(s) - \frac{1}{R}\Delta F(s) \ldots(3)$$

Where, $\Delta P_g(s)$ = governor output, $\Delta P_{ref}(s)$ = the reference signal, R = regulation constant or droop, $\Delta F(s)$ = frequency deviation due to speed

2.2.5 Load

The power systems load constitutes a diversity of electrical devices (Shouran, 2022). The resistive loads, for example, lighting and heating loads, are not dependent on frequency, but the motor loads are responsive to frequency, depending on the speed-load characteristics, as shown below:

$$\Delta P_e = \Delta P_L + D\Delta\omega \quad \ldots(4)$$

Where, ΔP_L = non-frequency responsive load change, $D\Delta\omega$ = frequency responsive load change, $D = \frac{\%change \in load}{\%change \in frequency}$

2.2.6 Tie-lines

Tie-lines link different areas in a power grid, facilitating power exchange between regions with varying frequencies (Xu et al., 2022). This exchange involves tie-line trades and synchronizing torque coefficients, leading to potential power errors. Tie-lines are designed for cost-effective power trading among neighboring systems and are essential when generating units experience power loss, aiding in frequency restoration.

Let there be two control areas, and power is to be exchanged from area 1 to area 2.

Mathematically,

$$P_{12} = \frac{|V_1||V_2|}{X_{12}} sin(\delta_1 - \delta_2) \quad \ldots(5)$$

Where, 1 stands for control area 1, and 2 stands for control area 2, X_{12}= series reactance involving areas 1 and 2, $|V_1|$ and $|V_2|$ = magnitude of voltages of area 1 plus area 2.

2.2.7 Area Control Error

LFC seeks to eliminate frequency errors across all areas and facilitate scheduled power exchanges via the tie-line. By correcting frequency errors to zero, it addresses steady-state tie-line power errors through area control error (ACE) signals, which each power-generating area employs (Masikana et al., 2024). To manage power interchange across various areas, LFC calculates real power flow through tie lines and subtracts predetermined interchange values to determine error levels (Roy & Oo, 2024). The total power exchange, jointly with a gain, B (MW/0.1Hz), known as the bias in frequency, as a multiplier with the divergence in frequency, is known as the Area Control Error (ACE) specified by,

$$ACE = \sum_{k=1}^{k} P_k - P_s + B(f_{act} - f_0)MW \quad \ldots(6)$$

Where, P_k = power in the tie line (if out of the area, then +ve), P_s = planned power exchange, f0 = base frequency, f_{act} = actual frequency. Positive (+ve) ACE shows that the flow is out of the area.

2.2.8 Parallel Operation of Generators

A parallel generator can be utilized for power generation in specific regions, showcasing its inertia constant, damping constant, and frequency response. The tie line flows and frequency droop illustrate the interconnection of power areas with varying governor-speed-droop characteristics (Nath & Sambariya, 2023). Effective power exchange necessitates synchronization at a common frequency. Figure 2 shows the block diagram for the parallel operation of generators.

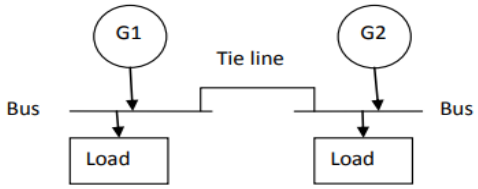

Figure 2: Block diagram for parallel operation of generators (Nath & Sambariya, 2023)

2.3 Modeling of LFC

This subsection covers the entire aspect of LFC design.

2.3.1 Modeling for the change in frequency

Let us consider a load frequency control loop of a system, which is isolated, intended for the examination of the steady state and dynamic responses, as shown in Figure 3.

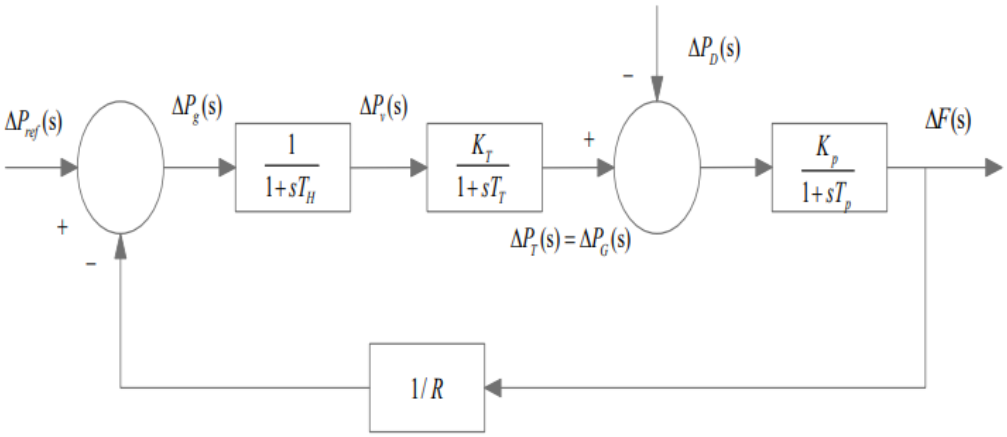

Figure 3: Load frequency control loop.

2.3.1.1 Steady state analysis

Let ΔP_{ref} be the setting for the speed changer and ΔP_D be the alteration in demand of the load. Considering a simple situation where the speed changer might have a constant setting,

i.e. $\Delta P_{ref} = 0$ as well as there is a change in the load demand. This may be known to be a free governor operation.

For such a process, the steady modification in the system frequency for a step change in load, i.e.

is obtained as follows:

$$\left[\left\{\Delta P_{ref}(s) - \frac{1}{R}\Delta F(s)\right\}\frac{K_T}{(1+sT_H)(1+sT_T)} - \Delta P_D(s)\frac{K_p}{(1+sT_p)} = \Delta F(s)\right] \quad \ldots(7)$$

This implies that,

$$\Delta F(s) = \frac{-K_p \Delta P_D(s)/s(1+sT_p)}{\left(\frac{K_T K_p}{R}\right)/(1+sT_H)(1+sT_T)(1+sT_p)} \quad \ldots(8)$$

After simplification, we get,

$$\Delta F(s) = \frac{-\Delta P_D}{\beta} \quad \ldots(9)$$

Where, β is the area frequency response characteristics

2.3.1.2 Dynamic analysis

For a step change in load,

$$\Delta F(s) = \frac{-K_p \Delta P_D(s)/s(1+sT_p)}{\left(\frac{K_T K_p}{R}\right)/(1+sT_H)(1+sT_T)(1+sT_p)} \quad \ldots(10)$$

Assuming amplifier and turbine response to be instantaneous, i.e., T_T=T_H=0 and K_T=1, we have

$$\Delta F(s) = \frac{-K_p}{(1+sT_p)+\frac{K_p}{R}}\frac{\Delta P_D}{s} \quad \ldots(11)$$

After simplification, we get,

$$\Delta F(s) = \frac{-RsK_p(1+sT_H)(1+sT_p)}{Rs(1+sT_H)(1+sT_T)(1+sT_p)+(s+RK_i)K_p}\frac{\Delta P_D(s)}{s} \quad \ldots(12)$$

2.3.2 Modeling of the Tie-Line

Let us consider that area 1 has surplus power and transfers power to area 2 by the tie-line. Figure 4 shows the Power transfer through the tie line.

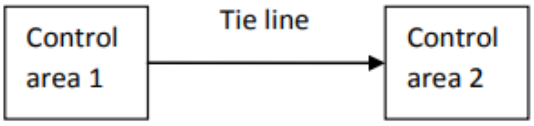

Figure 4: Power transfer through the tie line.

where, P_{12} is the power exchanged from area 1 towards area 2 via tie lines.

Then, the power transfer equation, the tie-line is specified as follows:

$$P_{12} = \frac{|V_1||V_2|}{X_{12}} sin(\delta_1 - \delta_2) \quad \ldots(13)$$

$$\Delta P_{12} = \frac{|V_1||V_2|}{X_{12}} cos(\delta_1 - \delta_2)(\Delta\delta_1 - \Delta\delta_2) \ldots(14)$$

Where, $\delta 1$ and $\delta 2$ are the power angles of end voltages and corresponding machines of the two Areas, X_{12}= reactance of the tie line, $|V_1|$ and $|V_2|$ = magnitude of voltages of area 1 plus area 2

The sequence of the subscripts depicts that the flow of power due to the tie lines is positive in the direction from 1 to 2.

For a little deviation in the angles $\delta 1$ and $\delta 2$ changes by $\Delta\delta 1$ and $\Delta\delta 2$, the tie line power changes as follows:

$$\Delta P_{12} = \frac{|V_1||V_2|}{X_{12}} cos(\delta_1 - \delta_2)(\Delta\delta_1 - \Delta\delta_2) \ldots(15)$$

i.e.

$$\Delta P_{12} = T^0(\Delta\delta_1 - \Delta\delta_2) \ldots(16)$$

i.e.

$$\Delta P_{12}(s) = \frac{2\pi T^0}{s}(\Delta F_1(s) - \Delta F_2(s)) \ldots(17)$$

Where, $T^0 = \frac{|V_1||V_2|}{X_{12}} cos(\delta 1 - \delta 2)$ = Torque produced …(18)

In a control area that is isolated, the incremental power (ΔPG – ΔPD) is the rate of rise of preserved kinetic energy due to a rise in the load, followed by a rise in the frequency. The power due to the tie-lines for each area is as follows:

$$\Delta P_1(s) = \Delta P_{12}(s) + a_{31}\Delta P_{31}(s) \ldots (19)$$

$$\Delta P_2(s) = \Delta P_{23}(s) + a_{12}\Delta P_{12}(s) \quad \ldots (20)$$

Control of tie line bias is utilized to get rid of the steady state error due to frequency, plus the exchange of power due to tie lines. This shows that all of the control areas should put in their share in frequency control, besides dealing with their particular total interchange of power.
Let ACE_1 = area control error of area 1, ACE_2 = area control error of area 2.
ACE_1, and ACE_2 are shown as linear arrangements of frequency along with tie-line power error as follows:

$$ACE_1 = \Delta P_{12} + b_1\Delta f_1 \quad \ldots (21)$$

$$ACE_2 = \Delta P_{23} + b_2\Delta f_2 \quad \ldots (22)$$

Where, b1 and b2, are known as biases in the area frequency of area 1, and area 2, respectively.
Area control error (ACE) is negative when the net power flow output from an area is very small or when the frequency has dropped, or both. During such situations, we need to increase the generation.

2.3.3 Modelling of a Single Area System

Figure 5 shows the Load Frequency Control (LFC) loop. The frequency, which changes with load, is contrasted with the reference speed setting. The frequency can be set to the desired value by making generation and demand equal with the help of a steam valve controller, which regulates the steam valve and increases power output from generators. It serves the primary/basic purpose of balancing the real power by regulating turbine output according to the variation in load demand (ΔP_0).

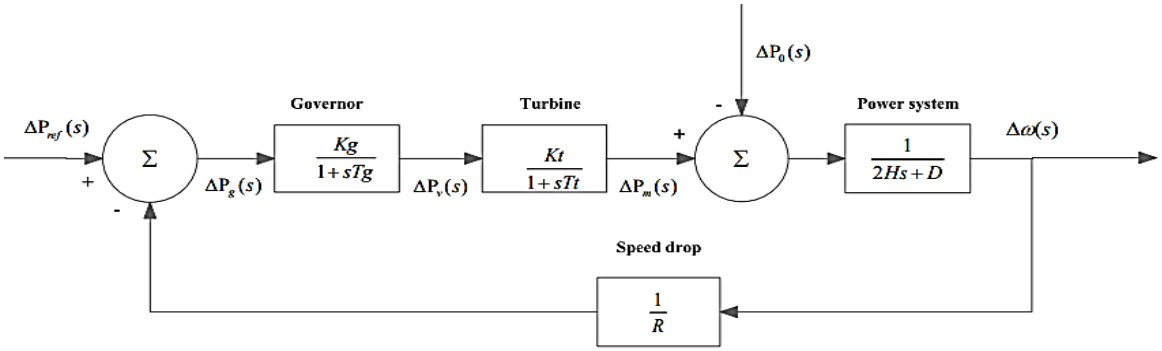

Figure 5: Model of a single-area LFC without using secondary control.

The transfer function of the model of the single area system, as shown in Eqn. (23):

$$KG(s)H(s) = \frac{1}{R}\frac{1}{(2Hs+D)(1+\tau_g s)(1+\tau_T s)} \ldots(23)$$

$$\frac{\Delta\omega(s)}{-\Delta P_L(s)} = \frac{(1+\tau_g s)(1+\tau_T s)}{(2Hs+D)(1+\tau_g s)(1+\tau_T s)+\frac{1}{R}} \ldots(24)$$

$$\Delta\omega(s) = -\Delta P_0(s)T(s) \ldots(25)$$

For the case with a load that is not sensitive to frequency load (D=0):

$$\Delta\omega_{ss} = (-\Delta P_0)R \ldots(26)$$

The integral controller, which is responsible for making the frequency deviation zero, is put in the secondary loop as shown in Figure 6.

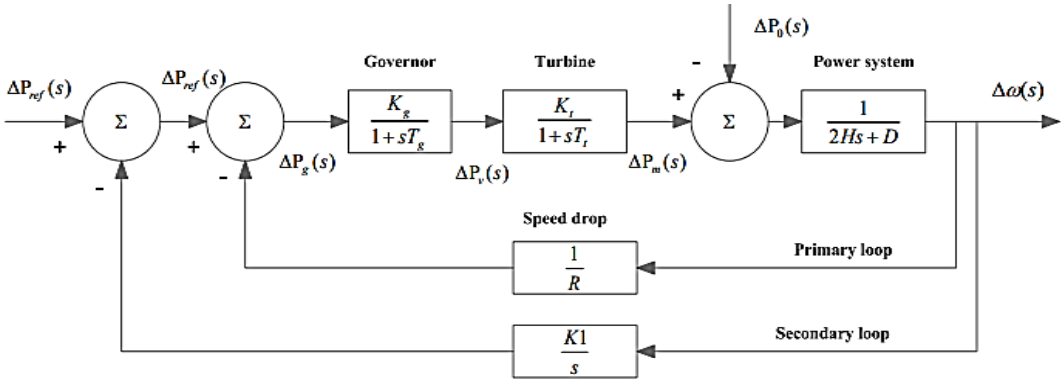

Figure 6: Model of single-area LFC using secondary control.

$$\omega = \frac{1}{D+\frac{1}{R}}\left[\Delta P_{ref} - \Delta P_0\right] \ldots(27)$$

2.3.4 Modelling of Two-Area System

Two area-interconnected systems, which are joined using tie-lines for the flow of tie-line power, may be described in the following equations. Let the additional input be $\Delta P12$, $\Delta P01$be the load change in area1 and the respective frequencies of the two areas be

$\Delta\omega = \Delta\omega_1 = \Delta\omega_2$28)

Let X_{12} be the reactance of the tie line, then the power delivered from area 1 to area 2 is

$P_{12} = \frac{|E_1||E_2|}{X_{12}} sin\delta_{12}$…(29)

The equation can be linearized as:

$\Delta P_{12} = \frac{dP_{12}}{d\delta_{12}} |\delta_{12}$…(30)

$\Delta\delta_{12} = P_s\Delta\delta_{12}$…(31)

The tie-line power deviation:

$\Delta P_{12} = P_s(\Delta\delta_1 - \Delta\delta_2)$…(32)

Let $\Delta\omega = \Delta\omega_1 = \Delta\omega_2$

For area 1,

$\Delta P_{m1} - \Delta P_{12} - \Delta P_{01} = \Delta\omega D_1$…(33)

$\Delta P_{m1} = -\Delta P_{m2} = \Delta P_{12} = \Delta\omega D_2$…(34)

For area 2,

$\Delta P_{m1} = \frac{-\Delta\omega}{R_1}$…(35)

$\Delta P_{m2} = \frac{-\Delta\omega}{R_2}$ …(36)

For an entire load change of the steady state, frequency deviation in two areas is as shown;

$\Delta\omega = \frac{-\Delta P_{L1}}{\left(\frac{1}{R_1}+D_1\right)\left(\frac{1}{R_2}+D_2\right)} = \frac{-\Delta P_{L1}}{\beta_1+\beta_2}$ …(37)

There can be one LFC for every control area in an interrelated multi-area system. ACEs are the actuating signals that stimulate modifications in reference power set points, such that $\Delta\omega$ becomes zero as soon as the steady-state is attained.

Each area ACE is a combination of frequency as well as tie-line error.

$$ACE_i = \sum nj = \Delta P_{ij} + K_i \Delta\omega \ldots(38)$$

2.4 Controller Design

The PID controller output is given as:

$$u(t) = K_p e(t) + K_i \int e(t)\, dt + K_d \frac{de(t)}{dt} \ldots(39)$$

Where:

K_p= proportional gain, K_i= integral gain, K_d= derivative gain, $e(t)$= Area Control Error (ACE)

2.5 Particle Swarm Optimization (PSO) for Controller Tuning

Particle Swarm Optimization (PSO) is a population-based optimization technique inspired by the social behavior of birds flocking or fish schooling. It is used in this study to optimally tune the PID controller parameters $(K_p, K_i, K_d)$to achieve improved system stability.

2.5.1 PSO Mathematical Formulation

Each particle represents a candidate solution defined as:

$$X_i = [K_p, K_i, K_d] \ldots(40)$$

The velocity and position of each particle are updated using:

$$v_i^{k+1} = wv_i^k + c_1 r_1 (pbest_i - x_i^k) + c_2 r_2 (gbest - x_i^k) \quad \ldots(41)$$

$$x_i^{k+1} = x_i^k + v_i^{k+1} \ldots(42)$$

Where:

w= inertia weight, c_1, c_2= cognitive and social coefficients, r_1, r_2= random numbers in [0,1], $pbest_i$= best position of particle i, $gbest$= global best position

2.5.3 Objective (Fitness) Function

The performance of each particle is evaluated using the Integral of Time-weighted Absolute Error (ITAE):

$$J = \int_0^T t \cdot (|\Delta f_1| + |\Delta f_2| + |\Delta P_{tie}|)\, dt \ldots(43)$$

The goal is to:

$\min J$ …(44)

This ensures reduced overshoot, faster settling time, and improved damping.

3.0 RESULTS AND DISCUSSION

3.1 Results of Frequency Deviation (Δf_1) in Area I

Figure 7 demonstrates the frequency deviation (Δf_1) responses in Area 1 for three controllers: Integral, classical PID, and PSO-optimized PID.

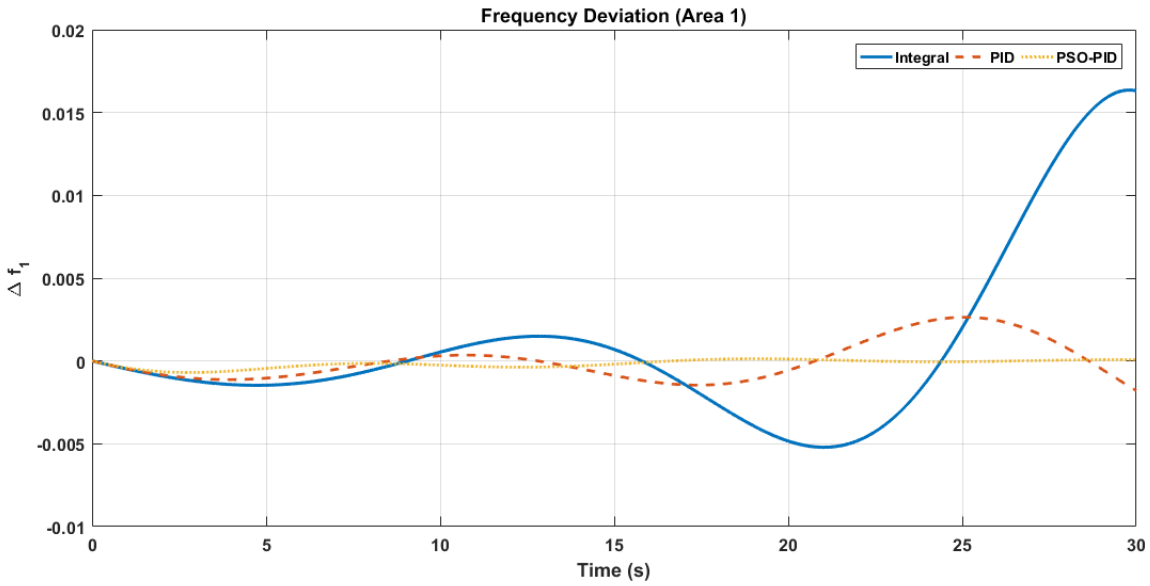

Figure 7: Area I Frequency Deviation. (Δf_1)

Initially, all controllers show minor negative deviations due to load disturbances, but their performances diverge significantly. The Integral controller has the weakest performance, leading to instability with increasing oscillations. The classical PID controller performs better with smaller undershoot and controlled oscillations but fails at complete stabilization. The PSO-optimized PID controller exhibits the most effective response, with minimal deviation and quick stabilization near zero, indicating robust resistance to disturbances. The analysis emphasizes the Integral controller's deficiencies and highlights the PSO-PID's effectiveness amid renewable energy challenges.

3.3 Results of Frequency Deviation (Δf_2) in Area II

Figure 8 analyzes the frequency deviation response (Δf_2) in Area II, influenced indirectly by tie-line interactions rather than direct load disturbances.

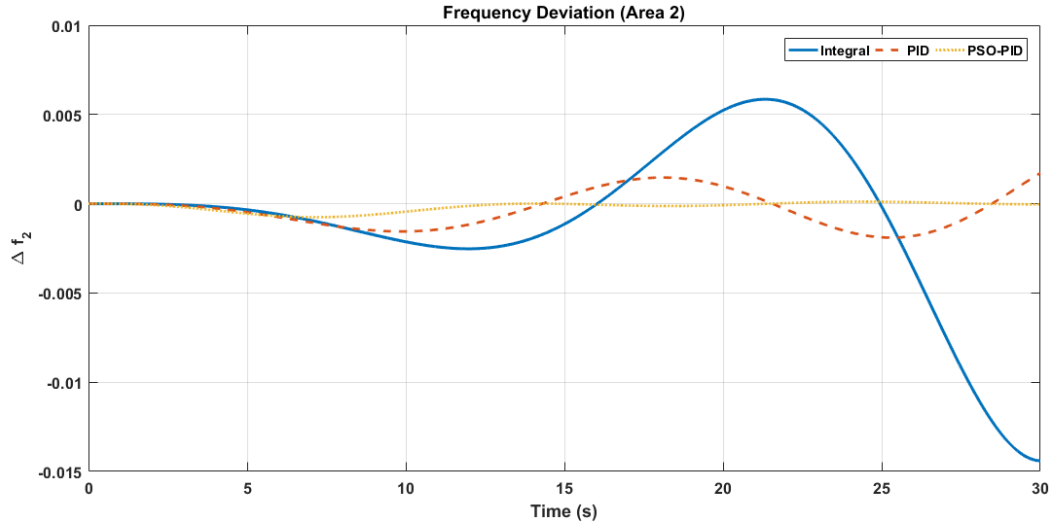

Figure 8: Area II Frequency Deviation (Δf_2).

Initial deviations in Area II are smaller than in Area I, indicating its stability. The Integral controller is ineffective, exhibiting increased oscillations and a significant negative peak of −0.014 Hz. In contrast, the classical PID controller performs better with reduced deviations and oscillations between −0.002 Hz and +0.0015 Hz, yet it still fails to stabilize fully. The PSO-optimized PID controller significantly outperforms others with near-zero frequency deviation and rapid stabilization, effectively managing disturbances, including those from renewable sources. The findings highlight the importance of coordinated control in interconnected power systems, especially as instability in Area I adversely impacts Area II.

3.4 Results of Tie-line power deviation (ΔP_{tie})

Figure 9 illustrates the tie-line power deviation (ΔP_{tie}) between Area I and Area II.

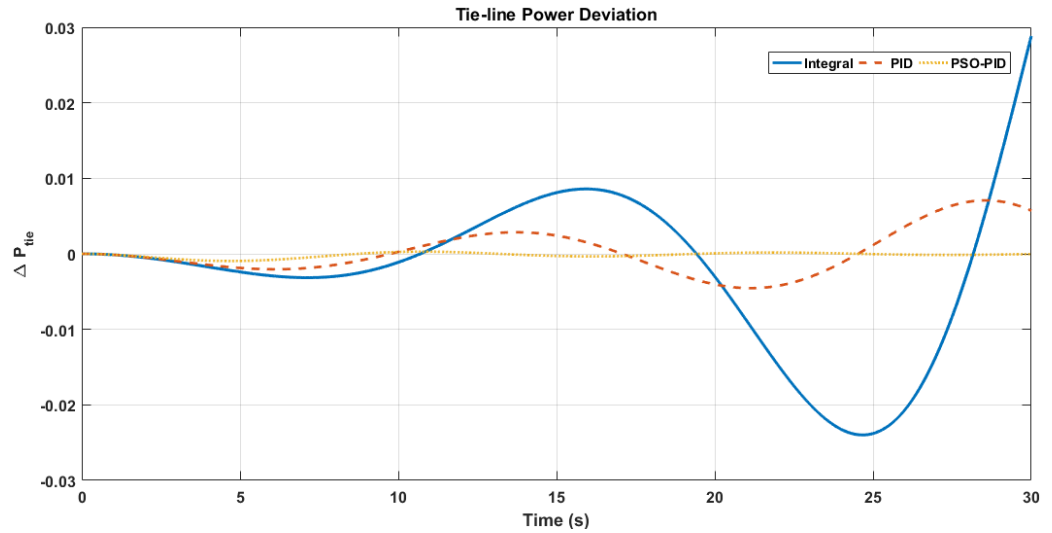

Figure 9: Tie-line power deviation. (ΔP_{tie})

This response highlights the coordination of power exchange in maintaining system stability after a disturbance. Initially, controllers show small deviations due to disturbances in Area 1. The Integral controller performs poorly, with significant oscillations in tie-line power, indicating inadequate control and potential system issues. The classical PID controller improves performance, reducing oscillations but still facing fluctuations. The PSO-optimized PID controller excels, maintaining near-zero response with quick damping of deviations, ensuring optimal power regulation and enhancing system reliability. While the Integral controller's instability risks power transfer and reliability, the PSO-PID controller effectively manages disturbances, including variability from renewable energy sources.

3.5 Performance comparison

Figure 10 shows the performance comparison of the three controllers using the selected key performance indicators.

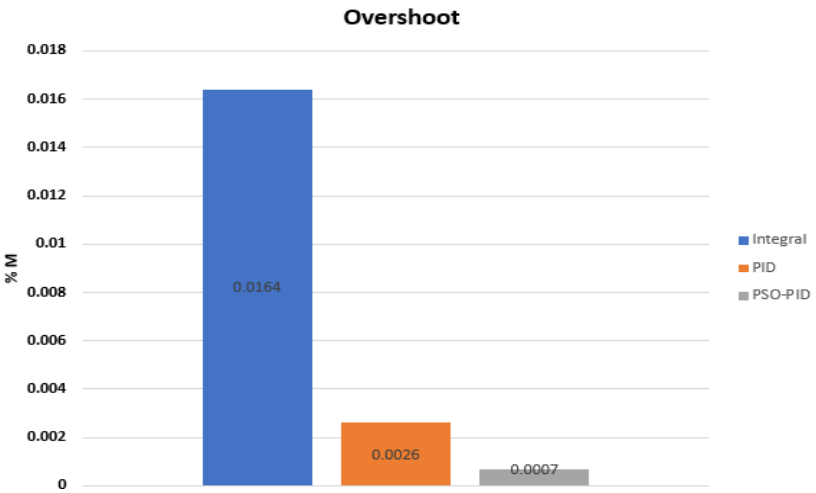

Figure 10: Overshoot ITAE of the controllers.

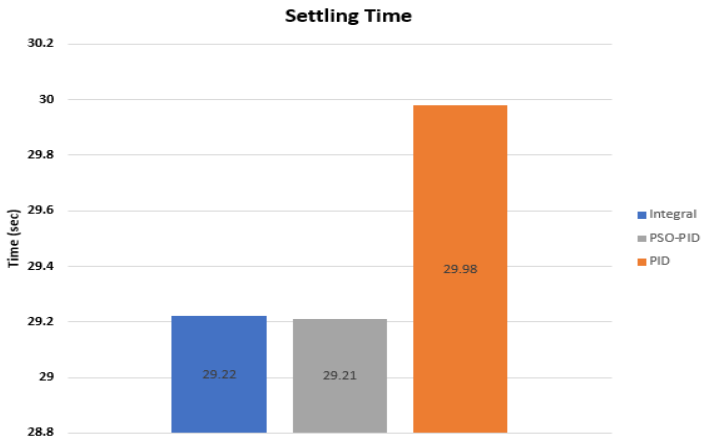

Figure 11: Settling time ITAE of the controllers.

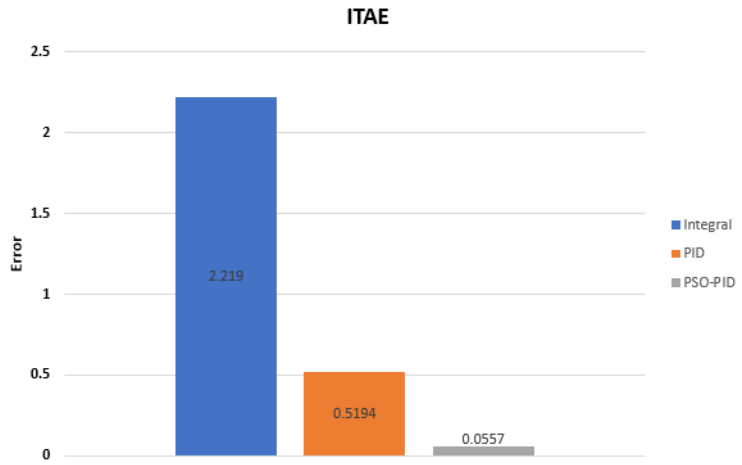

Figure 12: ITAE of the controllers.

From figure 10-12, the Integral controller demonstrates the weakest dynamic performance compared to the other controllers, with a notable overshoot of 0.0164 and a long settling time of 29.22 seconds, indicating a sluggish response. Additionally, it has the highest ITAE value of 2.2190, reflecting its difficulty in effectively dampening oscillations and addressing steady-state errors. This inefficiency results in extended deviations in system frequency, which is particularly problematic in applications like Load Frequency Control (LFC) where rapid stabilization is essential.

The PID controller outperforms the Integral controller, significantly reducing overshoot to 0.0026, indicating better damping and less oscillation. Although its settling time is slightly longer at 29.98 seconds, the ITAE value is much lower at 0.5194, showing effective minimization of time-weighted error. This enhancement is due to the integration of proportional, integral, and derivative components, improving both transient and steady-state performance.

The PSO-optimized PID (PSO-PID) controller shows superior performance, characterized by the lowest overshoot (0.0007) and the shortest settling time (29.21 s). Its ITAE value (0.0557) is significantly reduced, indicating effective error minimization. This demonstrates that Particle Swarm Optimization (PSO) enhances PID parameter optimization, balancing speed, stability, and accuracy.

3.6 DISCUSSION OF RESULTS

The evaluation of controller performance is based on key metrics such as overshoot, settling time, and Integral of Time-weighted Absolute Error (ITAE). The Integral controller displays poor performance with an overshoot of 0.0164, a settling time of 29.22 seconds, and a high

ITAE of 2.2190, indicating inefficiency in fast disturbance response. The PID controller significantly improves these metrics, achieving an overshoot of 0.0026, a slight increase in settling time to 29.98 seconds, and a reduced ITAE of 0.5194, showcasing balance in transient and steady-state performance. The PSO-PID controller outperforms both with an almost negligible overshoot of 0.0007, the fastest settling time at 29.21 seconds, and an ITAE of 0.0557, indicating exceptional efficiency in error minimization and disturbance rejection. Overall, transitioning from Integral to PID and further to PSO-PID controllers reflects substantial enhancements in system damping and stability, with the PSO-PID achieving the best overall performance.

3.7 CONCLUSION

In conclusion, the results clearly demonstrate that while conventional controllers such as Integral and PID provide acceptable performance, the adoption of intelligent optimization techniques like PSO leads to substantial improvements. The PSO-PID controller emerges as the most effective control strategy, offering superior dynamic response, enhanced stability, and optimal error minimization, making it a preferred choice for advanced Load Frequency Control applications in modern power systems.

3.8 RECOMMENDATION

The use of real-time simulators or hardware-in-the-loop platforms to test and validate control strategies under realistic operating conditions is recommended.

ACKNOWLEDGEMENT

Special appreciation goes to the Tertiary Education Trust Fund (TETFUND) for providing the opportunity to carry out this research work. The research with reference number (FPTB/TETF/DRD/CE/POLY/BAUCHI/IBR/2025/VOL. 1) is an important contribution as the output will be of immense significance in the areas of power system, and control. The efforts and contributions made by the Director, Directorate of Research and Development and his team in terms of assistance and guidance cannot be forgotten. Appreciation go to our colleagues for contributing their quota to the success of this research.

REFERENCES

1. Abdelghany, M. A., Syam, F. A., Aly, A. M., Abido, M. A., & Ibrahim, S. O. (2024). Load frequency and virtual inertia control for a power system using a fuzzy self-tuned PID controller with high penetration of renewable energy. *Journal of Electrical Systems and Information*

Technology, *11*(1). https://doi.org/10.1186/s43067-024-00173-x

2. Aditya Ranjan Buragohain, & Nipan Kumar Das. (2024). Load Frequency Control of a Single Area System Using a Fuzzy Logic Controller and Comparison with Integral and PID Controllers. *International Journal of Emerging Science and Engineering*, *12*(10), 7–11. https://doi.org/10.35940/ijese.f4511.12100924
3. Ahmed Oday, O., & Ahmed Jasim, S. (2021). AGC for Multi-Area Interconnected Using Computational Algorithm. *Journal of Hunan University Natural Sciences*, *48*.
4. Ali, J. S., Qiblawey, Y., Alassi, A., Massoud, A. M., Muyeen, S. M., & Abu-Rub, H. (2025). Power System Stability With High Penetration of Renewable Energy Sources: Challenges, Assessment, and Mitigation Strategies. *IEEE Access*, *13*(February), 39912–39934. https://doi.org/10.1109/ACCESS.2025.3546491
5. Alnefaie, S. A., Alkuhayli, A., & Al-Shaalan, A. M. (2025). Optimizing Load Frequency Control of Multi-Area Power Renewable and Thermal Systems Using Advanced Proportional–Integral–Derivative Controllers and Catch Fish Algorithm. *Fractal and Fractional*, *9*(6), 1–35. https://doi.org/10.3390/fractalfract9060355
6. Brahim, R. M. S., M'hamed, H., Taleb, R., & ... (2021). Load Frequency Control of a Hybrid Power System using Classical PID Controller. *IKSP Journal of Computer …*, 2021–2023. https://iksp.org/journals/index.php/ijcse/article/view/89%0Ahttps://iksp.org/journals/index.php/ijcse/article/download/89/93
7. Çavdar, B., Akyazi, Ö., Şahin, E., & Nuroğlu, M. (2024). Effect of PV Plant on Frequency Stability in IEEE12 Bus System for Different Penetration Levels and Depth of Frequency Support. *Arabian Journal for Science and Engineering*, *49*(12), 15899–15916. https://doi.org/10.1007/s13369-024-08733-z
8. Daood, O., Najeeb, M., & Ibrahim Ali, I. (2024). An Efficient Load Frequency Control for Multiple Power Systems Using Fuzzy Logic-Proportional Integral Derivative Controller. *International Journal of Electrical and Electronics Research*, *12*(2), 564–661. https://doi.org/10.37391/IJEER.120243
9. Dev, A., Léchappé, V., & Sarkar, M. K. (2021). Prediction-based super twisting sliding mode load frequency control for multi-area interconnected power systems with state and input time delays using a disturbance observer. *International Journal of Control*, *94*(7), 1751–1764. https://doi.org/10.1080/00207179.2021.1673487
10. Doan, D. V., Nguyen, K., & Thai, Q. V. (2021). A Novel Fuzzy Logic-Based Load Frequency Control for Multi-Area Interconnected Power Systems. *Engineering, Technology and Applied Science Research*, *11*(4), 7522–7530. https://doi.org/10.48084/etasr.4320
11. Elkasem, A. H. A., Kamel, S., Khamies, M., & Nasrat, L. (2024). Frequency regulation in a hybrid renewable power grid: an effective strategy utilizing load frequency control and redox

flow batteries. In *Scientific Reports* (Vol. 14, Issue 1). Nature Publishing Group UK. https://doi.org/10.1038/s41598-024-58189-2

12. Hamza, M., Buhari, M., & Sadiq, A. A. (2022). Modified PSO-Based Virtual Inertia Controller for Optimal Frequency Regulation of Micro-Grid. *COVENANT JOURNAL OF ENGINEERING TECHNOLOGY (CJET)*, *6*(2), 13–21.
13. Masikana, S. B., Sharma, G., & Sharma, S. (2024). Renewable energy sources integrated load frequency control of power system: A review. *E-Prime - Advances in Electrical Engineering, Electronics and Energy*, *8*(February), 100605. https://doi.org/10.1016/j.prime.2024.100605
14. Nath, V., & Samabriya, D. K. (2023). Investigating Load Frequency Control through Intelligent Controller Implementation for an Interconnected Power System. *Universal Journal of Electrical and Electronic Engineering*, *10*(4), 51–70. https://doi.org/10.13189/ujeee.2023.100401
15. Nath, V., & Sambariya, D. K. (2023). Application of an Intelligent controller For Load Frequency Control for Multi-Area Multi-Source Power System. *Indian Journal Of Science And Technology*, *16*(39), 3361–3374. https://doi.org/10.17485/ijst/v16i39.1769
16. Reddy, G. S., Srividhya, P., Poojitha, A., Manasa, Y., & Maheswari, V. S. U. (2024). Enhanced Load Frequency Control in Multi- Area Power Systems Using Fuzzy Logic Techniques. *Journal of Emerging Technologies and Innovative Research (JETIR)*, *11*(6), 349–358.
17. Roy, T. K., & Oo, A. M. T. (2024). Enhancing grid frequency regulation in low-inertia modern multi-area power systems using cascaded non-integer control approaches with BESS-based virtual inertia. *IET Renewable Power Generation*, *18*(S1), 4602–4620. https://doi.org/10.1049/rpg2.13169
18. Shouran, M. (2022). *Load Frequency Control for Multi-Area Interconnected Power System Using Artificial Intelligence Controllers*.
19. Wang, S., Bi, Y., Qi, W., Li, B., & Cai, K. (2021). Non-fragile load frequency control of a multi-area power system with an energy storage system and wind power subject to circular pole constraints. *Sustainable Energy Technologies and Assessments*, *45*(January), 101184. https://doi.org/10.1016/j.seta.2021.101184
20. Xu, K., Niu, Y., & Yang, Y. (2022). Load frequency control for wind-integrated multi-area power systems: An area-based event-triggered sliding mode scheme. *Journal of the Franklin Institute*, *359*(17), 9451–9472. https://doi.org/10.1016/j.jfranklin.2022.10.010